Rapid Communications

Schwinger scattering of twisted neutrons by nuclei

Andrei V. Afanasev,[1] D. V. Karlovets,[2] and V. G. Serbo[3,4]
[1]*Department of Physics, The George Washington University, Washington, D.C. 20052, USA*
[2]*Tomsk State University, Lenina Avenue 36, 634050 Tomsk, Russia*
[3]*Novosibirsk State University, RUS-630090 Novosibirsk, Russia*
[4]*Sobolev Institute of Mathematics, RUS-630090 Novosibirsk, Russia*

(Received 28 March 2019; revised manuscript received 5 September 2019; published 25 November 2019)

Thanks to Schwinger [Phys. Rev. **73**, 407 (1948)], the process of elastic scattering of neutrons by nuclei is known to depend on the interference between a nuclear amplitude and an electromagnetic one for small scattering angles, resulting in spin asymmetries of a cross section or in polarization of the scattered neutrons. Although this interference depends on the neutron's *transverse* polarization and on *an imaginary part* of the nuclear amplitude, this conclusion holds only for the incident plane-wave neutrons with a definite momentum. Here, we show that this scattering is altered when the twisted neutrons, recently obtained experimentally, are used instead—that is, neutrons with an orbital angular momentum. For bulk targets, the angular distributions of the scattered neutrons get modified, whereas scattering of a superposition of states with the different angular momenta also reveals dependence on the longitudinal polarization. For well-localized targets, the observables develop dependence on the neutron's *helicity* and on *a real part* of the nuclear amplitude, providing full access to its phase already in the Born approximation. We argue that the corresponding spin asymmetries are measurable at existing neutron facilities. Thus, scattering of the twisted neutrons by nuclei can provide means for quantum tomography of the neutron states and become a useful tool for hadronic studies, low-energy nuclear physics, tests of fundamental symmetries, and neutron optics.

DOI: 10.1103/PhysRevC.100.051601

Introduction. In 1948, Schwinger predicted that in a process of elastic scattering of the nonrelativistic neutrons by a nucleus with a charge Ze, the final neutrons become spin polarized, thanks to the spin-orbit coupling [1]. Nowadays, such a scattering is well studied, both theoretically [2] and experimentally [3], and the polarized cold and thermal neutrons are needed for a number of standard model test measurements (see, e.g., Ref. [4]).

The known properties of this scattering hold only for the plane-wave neutrons with a definite momentum. The rapid development of laser physics, of electron microscopy, and neutron optics recently allowed one to generate photons, electrons, and neutrons in the new quantum states [5–12], one of which is a so-called twisted state with a phase vortex and a corresponding orbital angular momentum projection onto a propagation direction [6,8,11,12]. In particular, the twisted cold neutrons with the energy of $E = 11$ meV and the wavelength of 0.27 nm were experimentally obtained at the Natural Institute of Standards and Technology [10], and methods for their generation were further developed in Ref. [13]. The twisted photons and electrons were shown to interact with the atoms, bulk materials, electromagnetic fields, and so on, different from the plane-wave beams due to a number of spin-orbit coupling phenomena, providing new tools for fundamental studies and applications [8,11,12]. It is of fundamental interest for the physics at mesoscopic scales to study new effects from the twisted neutrons, provided that ultracold neutrons with the wavelengths of 10–100 nm can be produced utilizing sequences of the magnetic quadrupoles [13,14].

In this Rapid Communication, we study how the Schwinger scattering is changed when the neutrons are twisted and identify several effects, absent with the ordinary neutron beams. Although the twisted neutron's wave function represents a superposition of plane waves, the resultant cross section cannot generally be represented as an incoherent mixture of the Schwinger cross sections. It is due to this quantum self-interference of the scattering amplitudes that, for the spatially localized targets, the observables develop dependence on the neutron's longitudinal polarization and on a real part of the nuclear amplitude (and, hence, on its phase)—the effects, inaccessible in the fully incoherent regime with a single beam of the delocalized plane-wave neutrons.

Importantly, we show that the scattering cross section becomes dependent on the nuclear amplitude's real part already in the Born approximation, in contrast to the Schwinger case; and this can be useful for studying the strong interaction at low energies where the perturbative quantum chromodynamics is not applicable. The use of the twisted neutrons for probing the complex nuclear amplitude for nonvanishing (but small—see below) scattering angles is complementary to such well-known methods as the neutron interferometry and the neutron gravity reflectometry, which result in similar phase sensitivity (see Refs. [4,15] and references therein). These features are somewhat analogous to those in scattering of the relativistic twisted electrons [16,17] and reveal themselves in the spin

asymmetries that can reach the values from 10^{-6} to 10^{-1}, which is detectable with the existing neutron facilities [2].

Scattering off a macroscopic target. Let the initial neutron first be in a plane-wave state with a momentum $\mathbf{p}$ and a wave-function $we^{i\mathbf{pr}/\hbar}$ where the spinor $w = w^{(\lambda)}(\mathbf{n})$ with a helicity λ is normalized as $w^\dagger w = 1$. The final neutron's wave function is $w'e^{i\mathbf{p}'\mathbf{r}/\hbar}$. We neglect the target recoil so that $p = p'$ and introduce the unit vectors $\mathbf{n} = \mathbf{p}/p$ and $\mathbf{n}' = \mathbf{p}'/p$ with the angles θ, φ and θ', φ'. The corresponding scattering amplitude is (see, for example, Ref. [18], Sec. 42)

$$f_{\lambda\lambda'}(\mathbf{n},\mathbf{n}') = w'^{\dagger}_{\lambda'}(a + i\mathbf{B}\boldsymbol{\sigma})w_\lambda, \quad \mathbf{B} = \beta\frac{\mathbf{n}\times\mathbf{n}'}{(\mathbf{n}-\mathbf{n}')^2},$$
$$\beta = \frac{\mu_n Z e^2}{m_p c^2} = -Z\times 2.94\times 10^{-16}\ \text{cm}, \qquad (1)$$

where $\boldsymbol{\sigma}$ are the Pauli matrices describing the neutron spin $\hat{\mathbf{s}} = \frac{1}{2}\boldsymbol{\sigma}$, $\mu_n = -1.91$, and m_p is the proton mass. Here, a is the nuclear amplitude whereas $i\mathbf{B}\boldsymbol{\sigma}$ relates to the electromagnetic interaction of the neutron's anomalous magnetic moment with a nucleus. For thermal neutrons with the energies near 25 meV and an $^{197}_{79}$Au nuclear target ($a = 7.63$ fm [19]), the relevant parameters are

$$\varepsilon \equiv |\beta/a| \approx 0.03, \quad |(\mathrm{Im}\, a)/a| \approx 2\times 10^{-4}. \qquad (2)$$

The standard (Schwinger) cross section summed over the spin states of the final neutrons and for the vector $\mathbf{n}$ directed along the z axis [i.e., $\mathbf{n} = \mathbf{e}_3 = (0,0,1)$] is

$$\frac{d\sigma^{(\mathrm{st})}(\mathbf{e}_3,\mathbf{n}',\boldsymbol{\zeta})}{d\Omega'} = |a|^2 + \frac{1}{4}[\beta\ \cot(\theta'/2)]^2 - \beta\zeta_\perp(\mathrm{Im}\, a)\cot(\theta'/2)\sin(\varphi'-\varphi_\zeta). \qquad (3)$$

The interference term depends on the transverse polarization of the initial neutron $\boldsymbol{\zeta}_\perp = \zeta_\perp(\cos\varphi_\zeta, \sin\varphi_\zeta, 0)$ but not on the longitudinal spin-polarization ζ_z or the helicity λ. For small scattering angles $\theta' \to 0$, the second term on the right-hand side has a Coulomb-like singularity of $(1/\theta')^2$, whereas the third term has a singularity $1/\theta'$.

Due to the time-reversal invariance, this single-spin correlation in (3) is the same for either initial or final neutron polarization, and the spin correlation averages to zero after the integration over the final neutron's azimuthal angle φ'. For higher energies at the Large Hadron Collider and Brookhaven National Laboratory Relativistic Heavy Ion Collider hadron colliders, a similar effect of the spin Coulomb-nuclear interference [20,21] provided a method to measure proton beam polarization at multi-GeV energies [22], presently known as "CNI polarimetry."

Now, we proceed to the twisted neutrons and use an approach developed in Ref. [23] for the twisted spinor particles. We assume that the incident twisted neutrons propagate along the quantization (z) axis and have the well-defined values of: (i) a longitudinal linear momentum p_z, (ii) an absolute value of a transverse momentum $|\boldsymbol{p}_\perp| \equiv \hbar\varkappa$, and (iii) a projection of a total angular momentum $J_z = m$, where m is a half-integer. Such *a Bessel state* has, moreover, a definite energy $E = (\hbar^2\varkappa^2 + p_z^2)/(2m_n)$ with m_n being the neutron mass and the helicity λ. The wave function is as follows:

$$\psi_{\varkappa m p_z\lambda}(\mathbf{r}) = \int \frac{d^2\mathbf{p}_\perp}{(2\pi)^2} a_{\varkappa m}(\mathbf{p}_\perp) i^\lambda w^{(\lambda)}(\mathbf{n}) e^{i\mathbf{pr}/\hbar}. \qquad (4)$$

Clearly, the function $\psi_{\varkappa m p_z\lambda}(\mathbf{r})$ can be considered as a coherent superposition of the plane-waves $w^{(\lambda)}(\mathbf{n})e^{i\mathbf{pr}/\hbar}$, weighted with the amplitude,

$$a_{\varkappa m}(\mathbf{p}_\perp) = i^{-m}e^{im\varphi}\frac{2\pi}{p_\perp}\delta(p_\perp - \hbar\varkappa). \qquad (5)$$

The momenta of these plane-wave components,

$$\mathbf{p} = (\mathbf{p}_\perp, p_z) = (\hbar\varkappa\cos\varphi, \hbar\varkappa\sin\varphi, p_z),$$

form a surface of a cone with an opening angle $\theta = \arctan(\hbar\varkappa/p_z)$.

Let us consider the scattering on a conventional thin-foil target, which we describe as an ensemble of atoms uniformly distributed over the large (compared to the beam's width) transverse extent; we call it *a macroscopic target*. If the target is thin so that one can neglect the neutrons' multiple scattering and attenuation, the scattering cross section can be obtained by the averaging over the atoms' positions in the target with respect to the beam axis. Such an averaged cross section represents an incoherent superposition of the standard ones (see Sec. B3 in Ref. [23]),

$$\frac{d\bar{\sigma}(\theta,\theta',\varphi',\boldsymbol{\zeta})}{d\Omega'} = \frac{1}{\cos\theta}\int_0^{2\pi}\frac{d\sigma^{(\mathrm{st})}(\mathbf{n},\mathbf{n}',\boldsymbol{\zeta})}{d\Omega'}\frac{d\varphi}{2\pi}. \qquad (6)$$

After the integration over the incoming neutron's azimuthal angle φ, we obtain [cf. Eq. (3)]

$$\frac{d\bar{\sigma}(\theta,\theta',\varphi',\boldsymbol{\zeta})}{d\Omega'} = \frac{1}{\cos\theta}[|a|^2 + \beta^2 G(\theta,\theta') - \beta(\mathrm{Im}\, a)\zeta_\perp g(\theta,\theta')\sin(\varphi'-\varphi_\zeta)],$$
$$G(\theta,\theta') = \frac{1}{2|\cos\theta - \cos\theta'|} - \frac{1}{4}, \qquad (7)$$
$$g(\theta,\theta') = \begin{cases}\cot(\theta'/2), & \text{at } \theta' > \theta,\\ -\tan(\theta'/2) & \text{at } \theta' < \theta.\end{cases}$$

This cross section is still independent of ζ_z, and it coincides with Eq. (3) in the limit $\theta \to 0$. Unlike the Schwinger cross-section (3), Eq. (7) has an angular singularity of $1/|\theta' - \theta|$ at $\theta' \to \theta$. This shift to the nonvanishing scattering angles can be useful for experimental analysis of the small-angle scattering. Indeed, thanks to this property the singular region is shifted from the small angles $\theta' \to 0$, which are difficult to access experimentally to the larger ones $\theta' \to \theta$, which can be controlled by the conical angle θ of the incoming neutrons.

In Fig. 1, we present the functions,

$$R_{\mathrm{em}} = \varepsilon^2 G(\theta,\theta'), \quad R_{\mathrm{int}} = \varepsilon g(\theta,\theta'), \qquad (8)$$

where R_{em} corresponds to a relative contribution of the electromagnetic interaction and R_{int} describes interference of the electromagnetic amplitude and the nuclear one. The magnitude of the asymmetry in this case is determined by an imaginary part of the nuclear amplitude $\mathrm{Im}(a)$ as in the original Schwinger's result, but the angular distribution is altered: The asymmetry experiences a steplike drop for the angles $\theta' \leqslant \theta$.

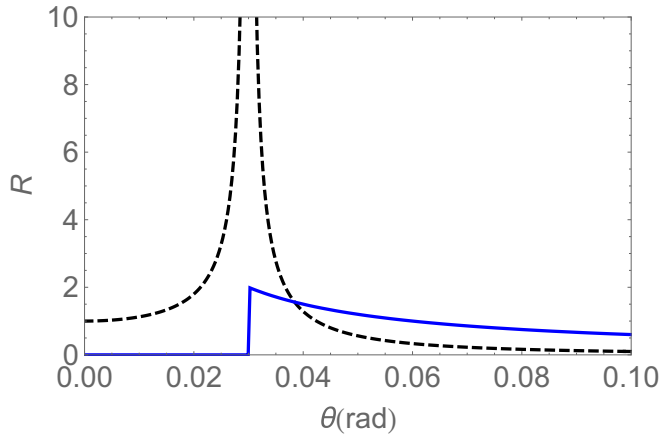

FIG. 1. The functions $R_{\rm em}$ (black dashed line) and $R_{\rm int}$ (blue solid line) from Eqs. (8) plotted vs the neutron-scattering angle θ' for $\theta = 0.03$ rad and $\varepsilon = 0.03$.

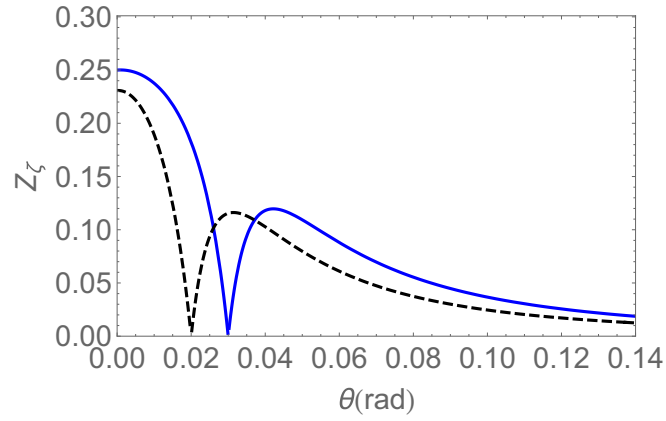

FIG. 2. The function Z_ζ defined from $|\langle\boldsymbol{\zeta}'\rangle| = \frac{|\mathrm{Im}\, a|}{|a|} Z_\zeta$ [cf. Eqs. (15) and (2)] plotted vs the neutron-scattering angle θ' for $\varepsilon = 0.03$, $2|c_1 c_2| = 1$, $\Delta m = 1$, $\theta = 0.03$ rad (blue solid line), and $\theta = 0.02$ rad (black dashed line).

A macroscopic target, a superposition of two Bessel beams. Let us take now a coherent superposition of two Bessel states with the different projections m_1 and m_2 but with the same helicity λ and the same beam axis. Such a superposition can be generated experimentally [10,13], and it is described by the following wave function:

$$\psi^{(2\,\mathrm{tw})}(\mathbf{r}) = c_1 \psi_{\varkappa m_1 p_z \lambda}(\mathbf{r}) + c_2 \psi_{\varkappa m_2 p_z \lambda}(\mathbf{r}),$$
$$c_n = |c_n| e^{i\alpha_n}, \quad |c_1|^2 + |c_2|^2 = 1. \tag{9}$$

With the help of this expression, we find

$$\frac{d\bar{\sigma}(\theta,\theta',\varphi',\boldsymbol{\zeta})}{d\Omega'} = \frac{1}{\cos\theta}\{\mathcal{A} + |c_1 c_2|[\beta^2\mathcal{B} + 2(\mathrm{Im}\, a)\beta(\boldsymbol{\zeta}\mathbf{C})]\},$$
$$\mathcal{A} = |a|^2 + \beta^2 G(\theta,\theta') + (\mathrm{Im}\, a)\beta(\boldsymbol{\zeta}\mathbf{e}_2) g(\theta,\theta'),$$
$$\mathcal{B} = \frac{\cos\gamma}{|c-c'|}[T(\theta,\theta')]^{|\Delta m|},$$
$$\mathbf{C} = \left[\frac{\Delta m}{|\Delta m|}\left(-\frac{c'}{s'}\mathbf{e}_1 + \mathbf{e}_3\right)\sin\gamma + \frac{c-c'}{|c-c'|}\mathbf{e}_2\cos\gamma\right][T(\theta,\theta')]^{|\Delta m|}, \tag{10}$$

where $s \equiv \sin\theta$, $c \equiv \cos\theta$, $s' \equiv \sin\theta'$, $c' \equiv \cos\theta'$, and

$$\gamma = (\varphi' - \pi/2)\Delta m + \Delta\alpha,$$
$$T(\theta,\theta') = \left(\frac{\tan(\theta/2)}{\tan(\theta'/2)}\right)^{\pm 1} \quad \text{for } \theta' \gtrless \theta,$$
$$\mathbf{e}_1 = (\cos\varphi', \sin\varphi', 0), \quad \mathbf{e}_2 = (-\sin\varphi', \cos\varphi', 0),$$
$$\mathbf{e}_3 = (0,0,1), \quad \mathbf{e}_i\mathbf{e}_k = \delta_{ik}. \tag{11}$$

In contrast to Eq. (7), derived for a single-m incident beam, this cross section depends on the differences of the total angular momenta $\Delta m = m_2 - m_1 \neq 0$ and of the states' phases $\Delta\alpha = \alpha_2 - \alpha_1$. This Δm and $\Delta\alpha$ dependence translates directly into the angular and polarization properties of the scattered neutrons. In particular:

(i) The cross section (10) depends not only on the neutron's transverse polarization $\boldsymbol{\zeta}_\perp$, but also on the longitudinal one ζ_z. It leads to the following longitudinal *polarization asymmetry*:

$$A_{\zeta_z} = \frac{d\bar{\sigma}(\zeta_z = +1) - d\bar{\sigma}(\zeta_z = -1)}{d\bar{\sigma}(\zeta_z = +1) + d\bar{\sigma}(\zeta_z = -1)} = \frac{2|c_1 c_2|(\mathrm{Im}\, a)\beta(\mathbf{C}\mathbf{e}_3)}{|a|^2 + \beta^2[G(\theta,\theta') + |c_1 c_2|\mathcal{B}]}, \tag{12}$$

which is on the order of $A_{\zeta_z} \approx 0.01\,\mathrm{Im}(a)/|a|$ for the scattering angles $\theta' \approx \theta$. For thermal neutrons and a gold target [see Eq. (2)], the predicted asymmetry amounts to *a few parts per* 10^6, which is in a range currently accessible for experiments on the hadronic parity violation [24] for which the above asymmetry may be a source of unwanted systematics, provided that the neutron beam becomes twisted due to uncontrolled interactions. However, as we show below, averaging over the azimuthal scattering angle φ' eliminates the dependence on ζ_z, which provides an approach to correct for this kind of systematics. Azimuthal angular coverage for the neutron-scattering detectors would be essential to deal with this systematic effect in parity-violation measurements.

(ii) The differential cross-section (10) averaged over the azimuthal angle φ' of the final neutron depends on $\boldsymbol{\zeta}_\perp$ and on $\mathrm{Im}\, a$ at $\Delta m = \pm 1$, but it is independent of the longitudinal polarization. It looks as follows:

$$\left\langle \frac{d\bar{\sigma}(\theta,\theta',\varphi',\boldsymbol{\zeta})}{d\Omega'} \right\rangle = \frac{1}{\cos\theta}[|a|^2 + \beta^2 G(\theta,\theta') + 2|c_1 c_2|(\mathrm{Im}\, a)\beta\boldsymbol{\zeta}\langle\mathbf{C}\rangle], \tag{13}$$

where

$$\langle\mathbf{C}\rangle = \frac{1}{2}\left(\frac{c'}{s'} - \frac{c-c'}{|c-c'|}\right)T(\theta,\theta')(\cos\Delta\alpha, \mp\sin\Delta\alpha, 0) \tag{14}$$

for $\Delta m = \pm 1$ and $\langle\mathbf{C}\rangle = 0$, otherwise. If the initial neutron is unpolarized, then its polarization after the

scattering is

$$\langle \boldsymbol{\zeta}' \rangle = 2|c_1 c_2| \frac{(\mathrm{Im}\, a)\beta}{|a|^2 + \beta^2 G(\theta, \theta')} \langle \mathbf{C} \rangle. \tag{15}$$

In Fig. 2, one can see that $|\langle \boldsymbol{\zeta}' \rangle| \approx 0.1 \frac{|\mathrm{Im}\, a|}{|a|}$ for $\theta \approx \varepsilon$, i.e., the predicted effect amounts to *tens of parts per* 10^6 for the thermal neutrons and the gold target [see Eq. (2)].

A single nucleus and a mesoscopic target. Let the single-m neutrons be scattered by a nucleus located on the transverse (xy) plane at a definite impact parameter $\mathbf{b} = (b_x, b_y, 0) = b(\cos\varphi_b, \sin\varphi_b, 0)$. Using the neutron's wave-function (4) and Eq. (1), we find the following scattering amplitude:

$$F^{(m)}_{\lambda\lambda'}(\theta, \theta', \varphi', \mathbf{b}) = i^{\lambda - m} e^{-i\mathbf{p}'_\perp \mathbf{b}/\hbar} \int_0^{2\pi} \frac{d\varphi}{2\pi} e^{im\varphi + i\mathbf{p}_\perp \mathbf{b}/\hbar} f_{\lambda\lambda'}(\mathbf{n}, \mathbf{n}'), \tag{16}$$

where the factor $\exp(i\mathbf{p}_\perp \mathbf{b}/\hbar)$ specifies the lateral position of the nucleus with respect to the beam. The angular distributions of the scattered neutrons can be obtained by squaring this amplitude; when summed up over the helicities and averaged over the azimuthal angle of the final neutrons, they can be expressed via the quantities $\mathbf{B}^{(\sigma)}(m, \varkappa, \mathbf{b}) = \int_0^{2\pi} \frac{d\varphi}{2\pi}$, $\mathbf{B} \exp\{i[(m - \sigma)\varphi + \varkappa b \cos(\varphi - \varphi_b)]\}$ and the Bessel function $J_n(z)$ as follows:

$$\begin{aligned}
W^{(m)}_\lambda(\theta, \theta', \mathbf{b}) &= \sum_{\lambda'} \left\langle \left| F^{(m)}_{\lambda\lambda'}(\theta, \theta', \varphi', \mathbf{b}) \right|^2 \right\rangle = \frac{1}{2}\Sigma^{(m)} + \lambda \Delta^{(m)}, \\
\Sigma^{(m)} &= |a|^2 \left[J^2_{m-1/2}(\varkappa b) + J^2_{m+1/2}(\varkappa b) \right] + \sum_\sigma \langle (\mathbf{B}^{(\sigma)*} \mathbf{B}^{(\sigma)}) - 2\sigma\, \mathrm{Im}(\mathbf{B}^{(\sigma)*} \times \mathbf{B}^{(\sigma)})_z \rangle, \\
\Delta^{(m)} &= \left[|a|^2 \cos\theta - (\mathrm{Re}\, a)\beta g(\theta', \theta) \sin\theta \right] \left[J^2_{m-1/2}(\varkappa b) - J^2_{m+1/2}(\varkappa b) \right] + \cos\theta \sum_\sigma \langle 2\sigma (\mathbf{B}^{(\sigma)*} \mathbf{B}^{(\sigma)}) - \mathrm{Im}(\mathbf{B}^{(\sigma)*} \times \mathbf{B}^{(\sigma)})_z \rangle \\
&\quad - \sin\theta \langle \mathrm{Im}(\mathbf{B}^{(1/2)*} \times \mathbf{B}^{(-1/2)})_x - \mathrm{Re}(\mathbf{B}^{(1/2)*} \times \mathbf{B}^{(-1/2)})_y \rangle,
\end{aligned} \tag{17}$$

where $\langle F \rangle = \int_0^{2\pi} \frac{d\varphi'}{2\pi} F(\varphi')$. As a result, we obtain a nonvanishing *helicity asymmetry*,

$$A_\lambda = \frac{W^{(m)}_{\lambda=1/2} - W^{(m)}_{\lambda=-1/2}}{W^{(m)}_{\lambda=1/2} + W^{(m)}_{\lambda=-1/2}} = \frac{\Delta^{(m)}}{\Sigma^{(m)}}. \tag{18}$$

In contrast to Eq. (3), the interference term in (17) depends on the initial neutron's helicity and on the real part of the nuclear amplitude (and, therefore, on its phase $\mathrm{Arg}\, a$), even after the azimuthal averaging. The angular distributions (17) are plotted in Fig. 3 for a $^{197}_{79}$Au nucleus as a function of its position $\varkappa b$. The scattering angle is chosen as $\theta' = 0.03$ rad for which the electromagnetic and strong amplitudes equally contribute to the cross section for the plane-wave neutrons. One can see that the former contribution dominates in the beam center ($b \to 0$) where the interference between two amplitudes is most pronounced. The asymmetry A_λ is a periodic function of $\varkappa b$ and of the amplitude's phase $\mathrm{Arg}\, a$; it can reach *tens of percent* even for a wider range of parameters than is shown in Fig. 4. Note that outside the cone opening angle, at $\theta' > \theta$, the sensitivity to the phase practically vanishes so that in order to probe both the real and the imaginary parts of the

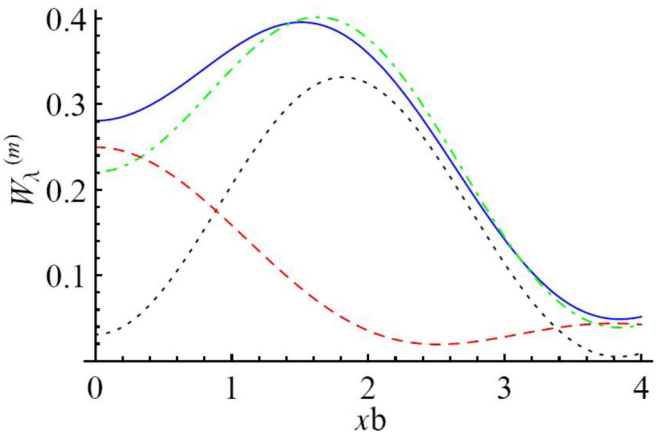

FIG. 3. The probability (17) as a function of the $^{197}_{79}$Au nucleus position $\varkappa b$ for $m = 1/2$, $\lambda = -1/2$, $\theta' = 0.03$, $\theta = 0.06$ rad, and $\varepsilon = 0.03$. The separate contributions from the nuclear amplitude (black dotted line) from the electromagnetic one (dashed red line), and the full result (solid blue line) are shown. The full result with an opposite sign of the strong amplitude (green dot-dashed line) demonstrates the role of its real part.

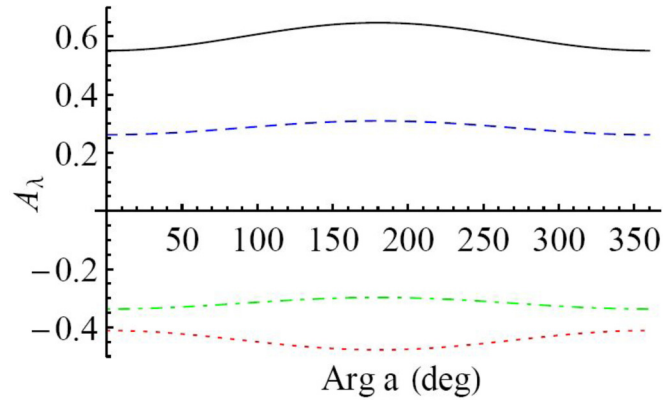

FIG. 4. The helicity asymmetry (18) for $\theta' = 0.03$, $\theta = 0.06$ rad, and $\varepsilon = 0.03$. Black line: $m = 1/2$, $\varkappa b = 0$, blue dashed line: $m = 1/2$, $\varkappa b = 1$, red dotted line: $m = 1/2$, $\varkappa b = 2$, green dot-dashed line: $m = 5/2$, $\varkappa b = 1$.

amplitude, one needs to perform measurements at the small angles $\theta' < \theta$, which is feasible.

When averaging over the impact parameters **b**, all the above features survive when the target is subwavelength sized or even if its width does not exceed that of the beam $1/\varkappa$ much (mesoscopic), whereas, for the macroscopic target, they vanish, see Eq. (7). Although for a single nucleus, the role of the amplitude's real part can be seen in Figs. 3 and 4 with the naked eye, the effect is additionally attenuated by the small parameter $1/(\varkappa\sigma_t) < 1$ for the mesoscopic target with the width $\sigma_t > 1/\varkappa$. For the Gaussian target with $\sigma_t \approx 1/\varkappa - 10/\varkappa$ and the angles $\theta' < \theta \approx 1^\circ$–$10^\circ$, the asymmetry reaches the values of

$$|A_\lambda| \approx 10^{-3}\text{–}10^{-1} \tag{19}$$

for a wide range of parameters.

Thus, scattering off the well-localized targets—say, of $\sigma_t \gtrsim$ 10–100 nm in width for the neutron wave packets with the wavelength of 0.1–100 nm and the transverse coherence length of $1/\varkappa \gtrsim 1$ nm $-$ 10 μm [13]—reveals dependence on the neutron's helicity and allows one to probe the nuclear amplitude's real part already in the Born approximation, whereas with a single beam of the delocalized plane-wave neutrons such a dependence arises beyond the tree level only. This method for high-precision measurements of the complex amplitude for nonvanishing scattering angles is alternative and complementary to the neutron interferometry and to the neutron gravity reflectometry.

Conventional Schwinger asymmetry can be enhanced for thermal neutrons due to the presence of nuclear resonances as was shown experimentally [25]. Extension of our formalism to the nuclear resonance region is straightforward in which case, we have to use appropriate parametrization for the nuclear amplitude a and use partial-wave expansion and angular integration in Eq. (16) in order to account for non-S-wave resonances.

Conclusion. Scattering outcomes generally depend on the projectiles' quantum states and their spatial profiles. The use of the twisted neutrons in the Schwinger process makes the observables dependent on the neutron's transverse momentum and—for well-localized targets—on its orbital momentum, the helicity, and on the phase of the nuclear amplitude. These spin-orbit-induced effects, absent with the ordinary neutrons in the Born approximation, allow one to develop tools for quantum tomography of the neutron beams and to study the complex nuclear amplitude as a function of the scattering angle and of the neutron energy. The predicted spin asymmetries range from 10^{-6} to 10^{-1} for realistic parameters and are detectable for existing neutron experiments aiming at much smaller numbers up to 10^{-8} [2].

The helicity asymmetries for the scattering of the plane-wave neutron (or electron) beams are used to study parity violation in the nuclear force [24]. The asymmetries predicted here do not violate parity as they correlate with the angular momentum, but the experimental methodology for studying the parity-violating scattering can also be used for the spin effects in the twisted-neutron scattering. Reliable estimates of these effects for specific experimental conditions require inclusion of the electron screening of the nuclear Coulomb field, similar to Ref. [2], which will be presented elsewhere.

Acknowledgments. We would like to thank D. Pushin, W. M. Snow, and A. Surzhykov for useful discussions. The work of D.V.K. and V.G.S. was supported by the Russian Science Foundation (Project No. 17-72-20013).

[1] J. Schwinger, Phys. Rev. **73**, 407 (1948).
[2] M. T. Gericke, J. D. Bowman, and M. B. Johnson, Phys. Rev. C **78**, 044003 (2008).
[3] C. G. Shull, Phys. Rev. Lett. **10**, 297 (1963).
[4] H. Rauch and S. A. Werner, *Neutron Interferometry*, 2nd ed. (Oxford University Press, Oxford, 2015).
[5] M. V. Berry and N. L. Balazs, Am. J. Phys. **47**, 264 (1979).
[6] L. Allen, M. W. Beijersbergen, R. J. C. Spreeuw and J. P. Woerdman, Phys. Rev. A **45**, 8185 (1992).
[7] G. A. Siviloglou, J. Broky, A. Dogariu, and D. N. Christodoulides, Phys. Rev. Lett. **99**, 213901 (2007).
[8] *Twisted Photons: Applications of Light with Orbital angular Momentum*, edited by J. P. Torres and L. Torner (Wiley-VCH, Weinheim, Germany, 2011).
[9] N. Voloch-Bloch, Y. Lereah, Y. Lilach *et al.*, Nature (London) **494**, 331 (2013).
[10] Ch. W. Clark, R. Barankov, M. G. Huber, M. Arif, D. G. Cory, and D. A. Pushin, Nature (London) **525**, 504 (2015).
[11] K. Y. Bliokh, I. P. Ivanov, G. Guzzinati, L. Clark, R. Van Boxem, A. Béchéd, R. Juchtmans, M. A. Alonso, P. Schattschneider, F. Nori, and J. Verbeeck, Phys. Rep. **690**, 1 (2017).
[12] B. A. Knyazev and V. G. Serbo, Phys.-Usp. **61**, 449 (2018).
[13] D. Sarenac, J. Nsofini, I. Hincks *et al.*, New J. Phys. **20**, 103012 (2018).
[14] D. Pushin (private communication).
[15] W. M. Snow, J. Apanavicius, K. A. Dickerson *et al.*, arXiv:1910.14271.
[16] I. P. Ivanov, D. Seipt, A. Surzhykov, and S. Fritzsche, Phys. Rev. D **94**, 076001 (2016).
[17] D. V. Karlovets, J. High Energy Phys. 03 (2017) 049.
[18] V. B. Berestetsky, E. M. Lifshitz, and L. P. Pitaevsky, *Quantum Electrodynamics* (Butterworth-Heinemann, Oxford, 1982), Vol. 4.
[19] V. F. Sears, Neutron News **3**, 26 (1992).
[20] B. Z. Kopeliovich and L. I. Lapidus, Sov. J. Nucl. Phys. **19**, 114 (1974); N. H. Buttimore, E. Gotsman, and E. Leader, Phys. Rev. D **18**, 694 (1978).
[21] G. Antchev, P. Aspell, I. Atanassov *et al.* (TOTEM Collaboration), Eur. Phys. J. C **76**, 661 (2016).
[22] J. Tojo *et al.*, Phys. Rev. Lett. **89**, 052302 (2002).
[23] V. Serbo, I. P. Ivanov, S. Fritzsche, D. Seipt, and A. Surzhykov, Phys. Rev. A **92**, 012705 (2015).
[24] B. R. Holstein, Nucl. Phys. A **737**, 85 (2004); M. J. Ramsey-Musolf and S. A. Page, Ann. Rev. Nucl. Part. Sci. **56**, 1 (2006).
[25] G. P. Felcher and S. W. Peterson, Acta Crystallogr., Sect. A: Cryst. Phys., Diffr., Theor. Gen. Crystallogr. **31**, 76 (1975).